LETTER TO THE EDITOR

Herschel⋆ observations of water vapour in Markarian 231

E. González-Alfonso[1], J. Fischer[2], K. Isaak[3], A. Rykala[3], G. Savini[4], M. Spaans[5], P. van der Werf[6], R. Meijerink[6], F. P. Israel[6], A. F. Loenen[6], C. Vlahakis[6], H. A. Smith[7], V. Charmandaris[8,21], S. Aalto[9], C. Henkel[10], A. Weiß[10], F. Walter[11], T. R. Greve[11,12], J. Martín-Pintado[13], D. A. Naylor[14], L. Spinoglio[15], S. Veilleux[16], A. I. Harris[16], L. Armus[17], S. Lord[17], J. Mazzarella[17], E. M. Xilouris[18], D. B. Sanders[19], K. M. Dasyra[20], M. C. Wiedner[21], C. Kramer[22], P. P. Papadopoulos[23], G. J. Stacey[24], A. S. Evans[25], and Y. Gao[26]

(Affiliations can be found after the references)

Preprint online version: May 21, 2010

ABSTRACT

The Ultra Luminous InfraRed Galaxy (ULIRG) Mrk 231 reveals up to seven rotational lines of water (H_2O) in emission, including a very high-lying ($E_{upper} = 640$ K) line detected at a 4σ level, within the Herschel/SPIRE wavelength range ($190 < \lambda(\mu m) < 640$), whereas PACS observations show one H_2O line at 78 μm in absorption, as found for other H_2O lines previously detected by ISO. The absorption/emission dichotomy is caused by the pumping of the rotational levels by far-infrared radiation emitted by dust, and subsequent relaxation through lines at longer wavelengths, which allows us to estimate both the column density of H_2O and the general characteristics of the underlying far-infrared continuum source. Radiative transfer models including excitation through both absorption of far-infrared radiation emitted by dust and collisions are used to calculate the equilibrium level populations of H_2O and the corresponding line fluxes. The highest-lying H_2O lines detected in emission, with levels at $300 - 640$ K above the ground state, indicate that the source of far-infrared radiation responsible for the pumping is compact (radius= $110 - 180$ pc) and warm ($T_{dust} = 85 - 95$ K), accounting for at least 45% of the bolometric luminosity. The high column density, $N(H_2O) \sim 5 \times 10^{17}$ cm^{-2}, found in this nuclear component, is most probably the consequence of shocks/cosmic rays, an XDR chemistry, and/or an "undepleted chemistry" where grain mantles are evaporated. A more extended region, presumably the inner region of the 1-kpc disk observed in other molecular species, could contribute to the flux observed in low-lying H_2O lines through dense hot cores, and/or shocks. The H_2O 78 μm line observed with PACS shows hints of a blue-shifted wing seen in absorption, possibly indicating the occurrence of H_2O in the prominent outflow detected in OH (Fischer et al., this volume). Additional PACS/HIFI observations of H_2O lines are required to constrain the kinematics of the nuclear component, as well as the distribution of H_2O relative to the warm dust.

Key words. Line: formation – Galaxies: ISM – Galaxies: individual: Markarian 231 – Infrared: galaxies – Submillimeter: galaxies

1. Introduction

One key question in the study of composite infrared (IR) merging galaxies and quasi-stellar objects (QSOs) is what fraction of their luminosity is generated in the nuclear region (< 200 pc) associated with the Active Galactic Nucleus (AGN) and a possible extreme nuclear starburst, and what fraction arises from a more extended kpc-scale starburst (e.g. Armus et al., 2007; Veilleux et al., 2009). The ULIRG Markarian 231 (Mrk 231) is the most luminous ($L \sim 4 \times 10^{12}$ L$_\odot$) galaxy in the local Universe ($z < 0.1$), and thus provides a unique template for such studies. Since the bulk of the luminosity in ULIRGs arises at far-IR wavelengths, where sub-arc-second resolution observations are not available, an alternative technique is required to constrain the compactness of the far-IR emission and its physical origin.

In a previous work based on observations with the *Infrared Space Observatory (ISO)*, González-Alfonso et al. (2008, hereafter G-A08) have argued that the observation of molecular species such as OH and H_2O at far-IR wavelengths is ideal for such a purpose, because their high-lying rotational levels are pumped through absorption of far-IR radiation and the observable excitation is then sensitive to the far-IR radiation density that in turn depends on the compactness of the far-IR contin-

uum source. In addition, these molecular observations shed light on the dominant chemistry in those nuclear regions. G-A08 reported the ISO detection of 3 high-lying H_2O lines, relevant upper limits over the entire ISO spectrum, and also high-lying OH lines, indicating the ocurrence of a compact-luminous far-IR component.

With their high sensitivity, spectral resolution, and wavelength coverage, the *Herschel* (Pilbratt et al., 2010) instruments are ideal for extending our previous study to additional key lines in the far-IR/submillimeter. As part of the HerCULES Key Programme (see van der Werf et al., 2010, this volume, hereafter vdW10), we report in this Letter the Herschel SPIRE/PACS (Griffin et al., 2010; Poglitsch et al., 2010) detection and first analysis of several H_2O lines in Mrk 231, which supports the conclusions of G-A08 and gives additional clues to the origin of H_2O in this ULIRG. We adopt a distance to Mrk 231 of 192 Mpc ($H_0 = 70$ km s^{-1} Mpc^{-1}, $\Omega_\Lambda = 0.73$, and $z = 0.04217$).

2. Observations

The SPIRE FTS observations of Mrk 231 (vdW10) were conducted on December 9th, 2009. The PACS observation of one H_2O line was conducted on November 8th, 2009, as part of the SHINING Key Programme, and kindly provided for the present study. Details on data reduction, calibration, and line extraction are given in vdW10 and Swinyard et al. (2010). Excerpts of the
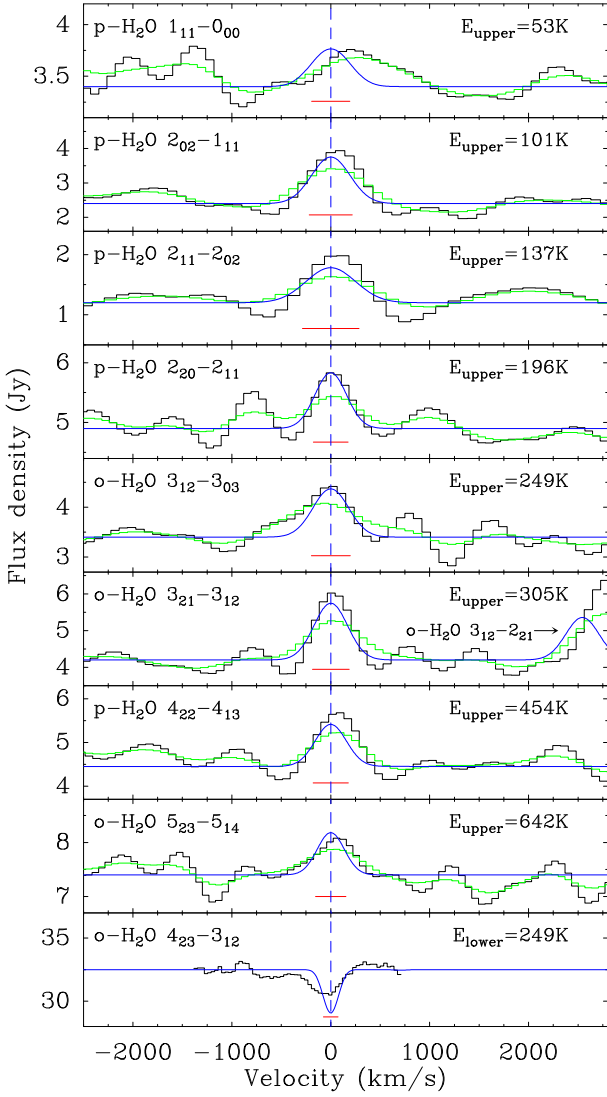
Fig. 1. Comparison between the observed spectra (black/green histograms: unapodized/apodized spectrum, see vdW10) and results for the reference model discussed in §3 (dark blue lines; a Gaussian instrumental line shape with FWHM = 0.048 cm^{-1} is used for simplicity). The $3_{12}2_{21}$ line, shown in the same panel as the $3_{21}3_{12}$ line, is blended with ^{12}CO (10-9) (vdW10). The red segment in each panel indicates the FWHM of an unresolved line. The velocity scale has been calculated with respect to the systemic redshift of $z = 0.04217$.

spectrum around the H_2O lines are displayed in Fig. 1, and an energy level diagram indicating the lines detected with SPIRE, the one detected with PACS, and those detected with ISO is shown in Fig. 2. Table 1 lists the line fluxes. Figure 1 also shows the results of our reference model, discussed below.

$H_2^{18}O$ could be marginally detected at 250.0 μm ($2_{20}2_{11}$) (see vdW10); however, this identification should be confirmed as the feature is shifted by 150 km s^{-1} from the nominal line wavelength. Confirmation of $H_2^{18}O$ would be important as its presence would support the strong enhancement of ^{18}O in Mrk 231 derived from ^{18}OH observations (Fischer et al., 2010, this issue, hereafter F10). A number of the H_2O lines in Fig. 1 are blended with the $C^{18}O$ lines $9-8$ (303.57 μm), $10-9$ (273.24 μm), and $11-10$ (248.43 μm). Contamination by $C^{18}O$ is minimal, however, as the lower-lying $6-5$, $7-6$, and $8-7$ lines are not
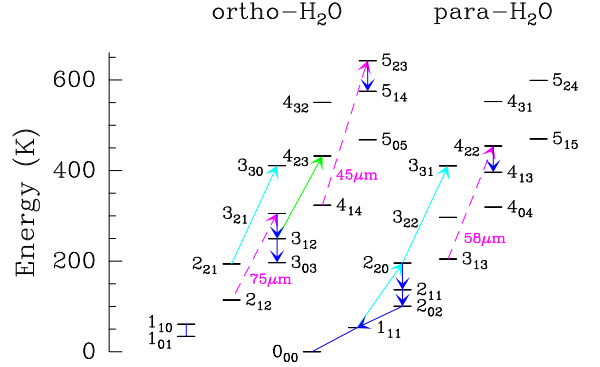

Fig. 2. Energy level diagram for H_2O, showing the detected/undetected (blue arrows/lines) lines with SPIRE, the line detected with PACS (green) and those detected by ISO (light blue). Dashed red arrows indicate the main pumping paths for the high-lying lines observed with SPIRE. Upward (downward) arrows: absorption (emission) lines.

detected. PACS observations show a broad absorption feature at 121.7 μm, nearly coincident with the H_2O $4_{32}4_{23}$ line (F10). However, this feature is probably contaminated by HF $(2-1)$ at the same wavelength, as the $1-0$ line is detected with SPIRE (vdW10); HF has been previously detected towards the Galactic star forming region Sgr B2 (Neufeld et al., 1997). Therefore the 121.7 μm feature is not used for the H_2O analysis below.

Of particular interest is the detection of the very high-lying $5_{23}5_{14}$ H_2O line at a 4σ level, which we have verified by reprocessing the data with no correction applied for the instrument spectral efficiency and by comparing these data with reduced observations of the dark sky over the same spectral range. The ground state lines (p-H_2O $1_{11}0_{00}$ in Fig. 1 and o-H_2O $1_{10}1_{01}$) are not detected. The lines detected with SPIRE are all in emission and peak at central velocities, in contrast to the low-lying OH lines that show P-Cygni profiles characteristic of an extreme molecular outflow (F10). The red horizontal lines indicate the FWHM of an unresolved line, and show that the H_2O lines detected with SPIRE are barely resolved. The o-H_2O $4_{23}3_{12}$ line detected with the higher spectral resolution of PACS is in absorption and well resolved, showing a central main body and, apparently, a relatively weak blue-shifted wing extending up to -800 km s^{-1} and possible low level emission from the receding gas. These wings should be confirmed with additional observations of H_2O absorption lines, as the limited wavelength coverage of the $4_{23}3_{12}$ line makes the adopted baseline uncertain. The detection would indicate that H_2O also participates in the prominent outflow detected in OH (F10).

While the shape of the $4_{23}3_{12}$ absorption line shows the centroid of the main body slightly blue-shifted (by ~ -70 km s^{-1}), some lines observed in emission tend to show, on the contrary, a slight red-shift of their centroid (up to 100 km s^{-1}). This effect could be related to systematic motions, i.e. a low-velocity nuclear-scale outflow, and will be explored in the future with additional high spectral resolution observations.

3. Analysis

The observed pattern of line emission cannot be explained in terms of *pure* collisional excitation (G-A08). Adopting the collisional rates of Faure et al. (2007) with $T_k > 200$ K[1] and $n(H_2) =$

---

[1] An LTE ortho-to-para H_2 ratio according to T_k is assumed.

Table 1. Observed and modeled line fluxes.

Line	λ (μm)	Flux[a] (Jy km s^{-1})	Model (Jy km s^{-1})
p-H$_2$O $\hat{1}$11000	269.27	< 300	177
o-H$_2$O $\hat{1}$10101	538.29	< 400	146
p-H$_2$O $\hat{2}$02111	303.46	718 (110)	660
p-H$_2$O $\hat{2}$11202	398.64	415 (43)	365
p-H$_2$O $\hat{2}$20211	243.97	342 (92)	372
o-H$_2$O $\hat{3}$12303	273.19	400 (130)	438
o-H$_2$O $\hat{3}$21312	257.79	631 (47)	657
p-H$_2$O $\hat{4}$22413	248.25	361 (38)	381
o-H$_2$O $\hat{5}$23514	212.53	287 (83)	269
o-H$_2$O $\hat{4}$23312	78.74	−910[b] (60)	−664

[a] Numbers in parenthesis indicate the estimated uncertainties.

[b] Includes the absorption in the high-velocity blue-shifted wing, which accounts for ~ -220 Jy km s^{-1}.

$10^6 - 10^7$ cm^{-3}, and ignoring radiative pumping, the models that account within a factor of 2 for the high-lying $\hat{5}$23514 and $\hat{4}$22413 lines predict fluxes for the low-lying lines that exceed the observed values by factors of $\gtrsim 10$. Thus the observed line ratios indicate an excitation mechanism that favours the emission in the high-lying ($\gtrsim 300$ K) lines at the expense of the low-lying lines. This does *not* imply that the H$_2$O lines are *not* formed in warm/dense regions, but just that the dominant excitation mechanism for the *high-lying* lines is not collisional.

Such a mechanism is the pumping through absorption of dust-emitted far-IR photons, which efficiently pumps the high-lying $\hat{3}$21312/$\hat{4}$22413/$\hat{5}$23514 lines through absorptions at 75.4/57.6/45.1 μm in the strong $\hat{3}$21212/$\hat{4}$22313/$\hat{5}$23414 lines (Fig. 2), of which the lower backbone levels are preferently populated. This requires a strong continuum component at $30 - 70$ μm. However, this component cannot dominate the emission at > 130 μm, as it would produce strong H$_2$O absorptions in that wavelength range that are not observed (G-A08). The data then support the occurrence of both a warm/compact component with moderate opacity, and a second colder component naturally associated with the more extended 1-kpc starburst that dominates the emission at long wavelengths. Our proposed SED decomposition is shown in Fig. 3a, and defines the *reference model* ($M_{\rm ref}$) with parameters as listed in Table 2: (*i*) a hot component (H_C) with $T_{\rm dust} = 150 - 400$ K dominates the emission at $\lambda < 20$ μm; (*ii*) a warm (95 K) and compact ($R = 120$ pc) component (W_C) dominates at $20\,\mu$m $< \lambda < 70\,\mu$m; (*iii*) an extended 1-kpc component (E_C), with $T_{\rm dust} = 40$ K, accounts for most of the continuum at $\lambda > 70$ μm. The W_C, with $L_W \sim 1.9 \times 10^{12}$ L$_\odot$, is responsible for the observed high-lying H$_2$O line emission.

Calculations for H$_2$O were carried out using the code described in González-Alfonso & Cernicharo (1999). In $M_{\rm ref}$ (Table 2), line broadening is caused by microturbulence. We have adopted a "mixed" approach (i.e. the H$_2$O molecules are evenly mixed with dust, G-A08), discussed below. An ortho-to-para H$_2$O abundance ratio of 3 is assumed. For those H$_2$O lines observed in emission, Fig. 3b compares the expected fluxes from the W_C (in violet) with the observed fluxes (in red). Collisional excitation is included with gas at $T_k = 150$ K and n(H$_2$) = 1.5×10^6 cm^{-3} but, even for these shock-like conditions[2], it has a

---

[2] The average densities are much lower than those adopted for collisional excitation, $<n$(H$_2$)$> \approx 200$ and 2000 cm^{-3} for E_C and W_C.
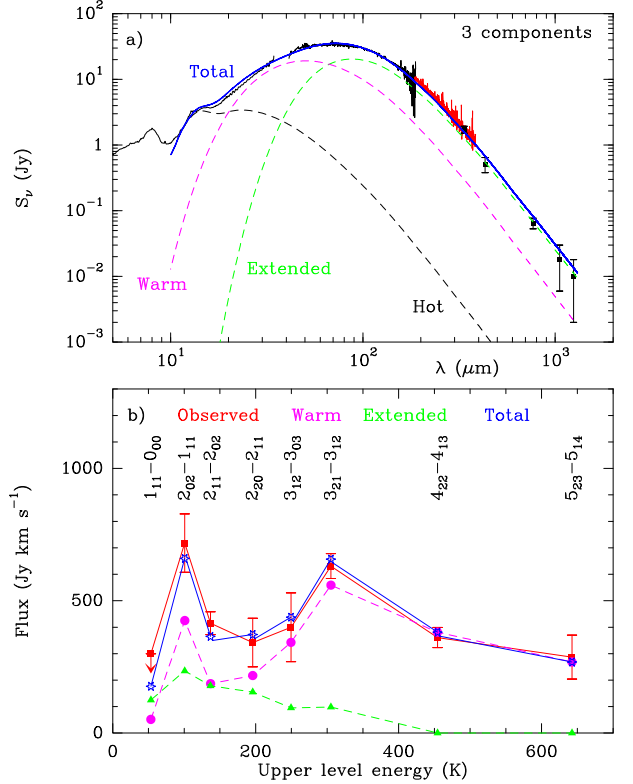

Fig. 3. Comparison between observations and results for the reference model. a) Continuum emission from Mrk 231. Spitzer IRS data (Armus et al., 2007), ISO data (G-A08), and SPIRE data (red spectrum) are shown. Flux densities at 800 and 1100 μm are taken from Roche & Chandler (1993, corrected for non-thermal emission), at 450 μm from Rigopoulou et al. (1996), and at 350 μm from Yang & Phillips (2007). b) H$_2$O emission. The high-lying lines are generated in the warm/compact region (violet), whereas the extended kpc-scale starburst (green) is expected to contribute to the low-lying lines.

low effect on the H$_2$O level populations and line fluxes as these are mostly determined by the strong radiation field. The high-lying lines are reproduced with the W_C, but there is a model deficit of emission from the low-lying lines. This deficit indicates that the E_C contributes to those low-lying lines (green); both radiative and collisional excitation, the latter significant for $E_{\rm upper} \leq 200$ K, are included in the model.

The high-lying $\hat{4}$22413 and $\hat{5}$23514 lines are (nearly) optically thin in the W_C, so that their expected fluxes are sensitive to N(H$_2$O). Table 2 shows that, despite the strong radiation field in this region, a high N(H$_2$O) is required to account for the observed fluxes. Assuming a gas-to-dust mass ratio of 100, the average H$_2$O abundance relative to H$_2$ in this W_C is 0.8×10^{-6}.

The H$_2$O line at 78.7 μm observed by PACS is consistently predicted in absorption, and its flux is reasonably reproduced (Table 1), given that the blue-shifted wing is not modeled. However, the observed line shape suggests systematic motions that are not included in our model. In general, we expect that lines with $\lambda \lesssim 120$ μm are observed in absorption, while lines with $\lambda \gtrsim 120$ μm are in emission (with exceptions due to the pumping details and level energies).

Concerning the ISO lines (G-A08), $M_{\rm ref}$ also matches the absorption in the $\hat{2}$20111 line at 101 μm, but underestimates the absorption in the $\hat{3}$30221 and $\hat{3}$31220 lines at 66.4 and 67.1 μm by a factor of 2. As mentioned above, our model uses a mixed

Table 2. Parameters of the reference model (M_{ref}).

Component→	Hot[a] (H_C)	Warm (W_C)	Extended (E_C)
Radius (pc)	23	120	610
T_{dust} (K)	400 − 150	95	41
$\tau_{100\mu m}$	0.4	1.0	0.5
L (L$_\odot$)	7.5×10^{11}	1.9×10^{12}	9.6×10^{11}
Gas Mass[b] (M$_\odot$)	1.9×10^{6}	5.9×10^{8}	7.7×10^{9}
$N(H_2O)$ (cm^{-2})	–	5.2×10^{17}	2.0×10^{16}
V_{turb} (km s^{-1})	–	60[d]	40
$n(H_2)$[c] (cm^{-3})	–	1.5×10^{6}	5×10^{5}
T_{gas}^{c} (K)	–	150	100

[a] The hot component does not contribute to the H$_2$O emission.
[b] A gas-to-dust mass ratio of 100 is assumed.
[c] These parameters are not well determined for W_C, as the excitation is dominated by radiative pumping.
[d] From Downes & Solomon (1998).

approach, which implies that for given values of $N(H_2O)$, the absorbing H$_2$O lines are relatively weak, as molecules located deep inside the source do not contribute to the absorption features. Conversely, if a screen approach is adopted (i.e. a H$_2$O shell surrounds the continuum source), the absorption lines become much stronger. In both approaches, the $N(H_2O)$ required to match the lines observed with SPIRE are similar. Thus an analysis that combines absorption and emission lines is a powerful tool to establish the distribution of H$_2$O relative to the warm dust responsible for the excitation. The screen version of M_{ref} yields absorption in $\hat{3}30221$, $\hat{3}31220$, and other transitions that overestimate the observed values or upper limits. Therefore, our preliminary result is that a combination of both the mixed and screen scenarios best describes that observed data, with the mixed version favoured. Nevertheless, it remains unclear what fraction of the observed $\hat{3}30221$ and $\hat{3}31220$ absorption arises from the outflow detected in OH (F10).

By increasing R_C, the radius of W_C, to 170 pc, and keeping L_W constant, the $\hat{3}21312/\hat{4}23312$ line strengths become overestimated by 50/25%, and the $\hat{2}11202/\hat{5}23514$ intensities are underestimated by 30%; given the simplicity of our spherically symmetric models, we estimate a size for W_C in the range $R_C = 110 − 180$ pc. A lower limit for the luminosity arising from W_C is estimated by decreasing T_{dust} to $85 − 80$ K and increasing $N(H_2O)$ to $\gtrsim 10^{18}$ cm^{-2}, which results in too weak $\hat{4}23312$ and ISO absorption lines. We estimate that the mid- and far-IR emissions from the nuclear region account for more than 45% of the bolometric luminosity; observations at $60 − 200$ μm are required to better constrain that value and to establish a firm upper limit. Results are more uncertain for E_C, and we may expect that its contribution to the H$_2$O emission arises from its innermost region.

4. Discussion

The extreme nature of the nuclear region in Mrk 231 is well illustrated by comparing its SPIRE spectrum with that of the Orion Bar (Habart et al., 2010, this issue), the prototypical Galactic PDR. The Orion Bar spectrum shows CO lines a factor of $\gtrsim 50$ stronger than the H$_2$O lines, while in Mrk 231 the H$_2$O and CO lines have comparable strengths (vdW10). This contrast will be still higher in the nuclear region, provided that a significant fraction of the CO emission in Mrk 231 arises from a more extended region. Thus the H$_2$O-to-CO line intensity ratios in the SPIRE

wavelength range are an excellent diagnostic of extragalactic compact/warm far-IR continuum sources with unusually high amounts of H$_2$O.

The above comparison also indicates that the nuclear region of Mrk 231 cannot be interpreted as an ensemble of classical PDRs. Three main scenarios are proposed to explain such high amounts of H$_2$O: (*i*) widespread shocks/cosmic rays: although the H$_2$O lines peak around the systemic velocity, outflows of ~ 100 km s^{-1} are not ruled out by our data, and indeed some indications in the H$_2$O line shapes of systematic motions have been found; an enhanced cosmic ray flux could also have an important impact on the nuclear chemistry. (*ii*) XDR chemistry: our derived H$_2$O abundance of $\sim 10^{-6}$ is in very good agreement with XDR model results by Meijerink & Spaans (2005, their Fig. 3, Model 3), as well as with our preliminary estimate of the H$_2$O spatial distribution. (*iii*) An undepleted chemistry, where H$_2$O that formed on grain mantles is released into the gas phase, as in Galactic hot cores; in support of this scenario, the derived T_{dust} in W_C is close to the evaporation temperature of solid H$_2$O. All three scenarios are probably taking place, and the identification of the dominant process requires a multi-species analysis.

The nuclear region traced by the high-lying H$_2$O lines has a size similar to the nuclear disk (or outflow) observed at radio wavelengths and H I 21 cm by Carilli et al. (1998, their Figs. 3 & 7), suggesting a close physical correspondence. From H_C and W_C, the nuclear surface brightness ($\sim 1.5 \times 10^{13}$ L$_\odot$ kpc^{-2}) exceeds the highest values attained in starburst on spatial scales $\gtrsim 100$ pc (Meurer et al., 1997; Davies et al., 2007), while the nuclear luminosity-to-mass ratio ($L/M \sim 4 \times 10^{3}$ L$_\odot$/M$_\odot$) exceeds the limit for a starburst estimated by Scoville (2003). From near-IR data, Davies et al. (2007) estimated a starburst luminosity from a similarly sized region of $\lesssim 7 \times 10^{11}$ L$_\odot$; according to the joint luminosity of our H_C and W_C, the AGN would account for at least 50% of the output power in Mrk 231.

References

Armus, L., Charmandaris, V., Bernard-Salas, J., et al. 2007, ApJ, 656, 148
Carilli, C. L., Wrobel, J. M., & Ulvestad, J. S. 1998, ApJ, 116, 1007
Davies, R. I., et al. 2007, ApJ, 671, 1388
Downes, D., & Solomon, P.M. 1998, ApJ, 507, 615
Faure, A., et al. 2007, AA, 472, 1029
Fischer, J., et al. 2010, this volume (F10)
González-Alfonso, E., & Cernicharo, J. 1999, ApJ, 525, 845
González-Alfonso, E., Smith, H. A., et al. 2008, ApJ, 675, 303 (G-A08)
Griffin, et al. 2010, AA, this volume
Habart, E., et al. 2010, this volume
Meijerink, R., & Spaans, M. 2005, AA, 436, 397
Meurer, G.R., Heckman, T.M., Lehnert, M.D., Leitherer, et al. 1997, AJ, 114, 54
Neufeld, D. A., Zmuidzinas, J., Schilke, P., et al. 1997, ApJ, 488, L141
Pilbratt, et al. 2010, AA, this volume
Poglitsch, et al. 2010, AA, this volume
Rigopoulou, D., Lawrence, A., & Rowan-Robinson, 1996, MNRAS, 278, 1049
Roche, P.F., & Chandler, C.J. 1993, MNRAS, 265, 486
Scoville, N. 2003, J. Korean. Astron. Soc., 36, 167
Swinyard, B., et al. 2010, this volume
van der Werf, P., et al. 2010, this volume (vdW10)
Veilleux, S., et al. 2009, ApJS, 182, 628
Yang, M., & Phillips, T. 2007, ApJ, 662, 284

[1] Universidad de Alcalá de Henares, Departamento de Física, Campus Universitario, E-28871 Alcalá de Henares, Madrid, Spain

[2] Naval Research Laboratory, Remote Sensing Division, Washington, DC 20375, USA

[3] ESA Astrophysics Missions Div/ Research and Scientific Support Dept ESTEC/SRE-SA Keplerlaan 1, NL-2201 AZ Noordwijk, The Netherlands

[4] Department of Physics & Astronomy, University College London, Gower Street, London WC1E 6BT ,UK

[5] Kapteyn Astronomical Institute, University of Groningen, P.O. Box 800, 9700 AV, Groningen, the Netherlands

[6] Leiden Observatory, Leiden University, P.O. Box 9513, 2300 RA Leiden, The Netherlands

[7] Harvard-Smithsonian Center for Astrophysics, 60 Garden Street, Cambridge, MA 02138, USA

[8] University of Crete, Department of Physics, GR-71003, Heraklion, Greece

[9] Onsala Space Observatory, Chalmers University of Technology, 439 92 Onsala, Sweden

[10] MPIfR, Auf dem Hügel 69, 53121 Bonn, Germany

[11] Max-Planck-Institut für Astronomie, Königstuhl 17, D-69117 Heidelberg, Germany

[12] Dark Cosmology Centre, Niels Bohr Institute, University of Copenhagen, Juliane Maries Vej 30, 2100 Copenhagen, Denmark

[13] Centro de Astrobiología (CSIC-INTA), Ctra de Torrejón a Ajalvir, km 4, 28850 Torrejón de Ardoz, Madrid, Spain

[14] Space Astronomy Division, Institute for Space Imaging Science, Department of Physics and Astronomy, University of Lethbridge, Lethbridge, Alberta Canada, T1K 3M4

[15] Istituto di Fisica dello Spazio Interplanetario, CNR via Fosso del Cavaliere 100, I-00133 Roma, Italy

[16] Department of Astronomy, University of Maryland, College Park, MD 20742 USA

[17] IPAC, California Institute of Technology, MS 100-22, Pasadena, CA 91125, USA

[18] Institute of Astronomy and Astrophysics, National Observatory of Athens, P. Penteli, GR-15236 Athens, Greece

[19] University of Hawaii, Institute for Astronomy, 2680 Woodlawn Drive, Honolulu, HI 96822, USA

[20] Laboratoire AIM, CEA/DSM - CNRS - Université Paris Diderot, Irfu/Service d'Astrophysique, CEA Saclay, Orme des Merisiers, 91191 Gif sur Yvette Cedex, France

[21] LERMA, Observatoire de Paris, CNRS, 61 Av. de l'Observatoire, 75014 Paris, France

[22] Instituto Radioastronomia Milimetrica (IRAM), Av. Divina Pastora 7, Nucleo Central, E-18012 Granada, Spain

[23] Argelander Institut fuer Astronomy, Auf dem Huegel 71, D-53121, Germany

[24] Department of Astronomy, Cornell University, Ithaca, NY, USA

[25] Department of Astronomy, University of Virginia, 530 McCormick Road, Charlottesville, VA 22904, USA

[26] Purple Mountain Observatory, Chinese Academy of Sciences, 2 West Beijing Road, Nanjing 210008, China